ASME Journal of Autonomous Vehicles and Systems
Online journal at:
https://asmedigitalcollection.asme.org/autonomousvehicles

Prescribed Performance Backstepping and Sliding Mode Control for Automated Platoons With Internal Type-2 Fuzzy Logic and Exponential Spacing Policy

Natnael M. Negash
Mechanical Engineering,
Texas Tech University,
805 Boston Ave.,
Lubbock, TX 79409
e-mail: natnael.m.negash@ttu.edu

Shu-Xia Tang
Mechanical Engineering,
Texas Tech University,
805 Boston Ave.,
Lubbock, TX 79409
e-mail: shuxia.tang@ttu.edu

James Yang[1]
Mechanical Engineering,
Texas Tech University,
805 Boston Ave.,
Lubbock, TX 79409
e-mail: james.yang@ttu.edu

This study presents a control strategy employing a hybrid backstepping and sliding mode control (BSMC) approach for automated platoons. The control scheme integrates an exponential spacing policy tailored to varying driving conditions and vehicle constraints. We introduce an interval type-2 fuzzy logic system (IT2FLS) to approximate the unknown nonlinear driving resistance term. This technique yields interval outputs, incorporating uncertain mean and standard deviation in the membership functions of inputs, thereby enhancing the system's adaptability. We include a prescribed performance control using an asymmetric prescribed performance function to ensure string stability and confine spacing errors within a desired range. This technique eliminates the need for complex Laplace transform computations to check string stability. To validate the robustness of the proposed controller, we conduct simulations under fault and fault-free conditions, demonstrating the efficacy of the proposed approach. [DOI: 10.1115/1.4066315]

Keywords: automated platoon, IT2FLS, exponential spacing policy, backstepping and sliding mode control, prescribed performance, string stability, actuator fault

1 Introduction

Intelligent transportation systems will solve numerous traffic and energy inefficiencies in the coming years. Advanced expert and optimal control algorithms and wireless communication technologies enable the potential revolution of smart cities through automated vehicles (AVs) and modern road infrastructures. Automated platooning represents an intelligent technology in which AVs are interconnected through vehicle-to-vehicle (V2V) wireless communication and maintain optimal inter-vehicle spacing and velocity based on real-time traffic demands. This approach substantially alleviates traffic congestion, instability, fuel inefficiency, and road safety [1–5].

The design of the control system for such an automated platoon should achieve the objective of guaranteeing individual stability and string stability (SS) criterion under particular information flow topologies (IFTs) and desired spacing policies (SP). String stability (SS) denotes the desired condition where spacing errors among individual vehicles do not propagate downstream within the platoon string [6]. IFTs denote how information can be transferred among the AVs through V2V communication [7]. Some of these IFTs are predecessor following (PF), bidirectional (BD), bidirectional leader (BDL), predecessor leader-follower (PLF), two-predecessor follower, and two-predecessor leader-follower. In the PF topology, the follower vehicle receives information from the leader and predecessor vehicles, whereas in the BD case, the vehicle receives information from the predecessor and its follower. The SP represents the desired inter-vehicle spacing during the following scenario. These include constant-distance gap policy (CDGP) [8,9], constant-time gap policy (CTGP) [10], variable-time headway policy [11], safety spacing policy (SSP) [12], and nonlinear spacing policies [13,14]. The nonlinear SPs include quadratic spacing policy (QSP), improved QSP, etc. Moreover, the vehicle model or the node dynamics (ND) is utilized to develop the control algorithm. The ND can be a second-order or third-order model, and it can also be linear or nonlinear.

The feedback control laws, which rely on the abovementioned IFTs and SP, denote the cooperative control algorithms employed to stabilize the whole vehicle string. Many linear and nonlinear control algorithms were proposed to accomplish the corresponding control objectives, as in Refs. [15–26]. Another important thing to mention is the approximation of the unknown nonlinear terms and unknown exogenous disturbances. Practically, the vehicles are subjected to unknown resistance forces, actuator faults, and communication delays. Hence, fault-tolerant controls and powerful approximation techniques support the main controllers in achieving asymptotic tracking while the vehicle is subjected to unknown resistances and random actuator faults. Even though the development of such controls upholds some realistic assumptions, current studies

[1]Corresponding author.

Manuscript received November 29, 2023; final manuscript received August 15, 2024; published online September 13, 2024. Assoc. Editor: Sergey Nersesov.

usually consider a few of the assumptions to simplify the burden associated with stability proof and mathematical computation.

Peng [27] implemented an intelligent, robust backstepping control (BC) for vehicular platoon control. In the paper, he proposed an output recurrent cerebellar model articulation to mimic the ideal BC to compensate for the unknown uncertainty and disturbance. The study used a CDGP and did not incorporate actuator faults or achieve strong SS of the platoon. Chou et al. [28] proposed the BC method to regulate the time gap of individual vehicles of a homogeneous platoon. To prevent the explosion of terms, dynamic surface control with damping was fuzed with the controller. In the study, third-order nonlinear ND with CTGP was employed. A mechanism for achieving the strong SS of the platoon was not stated. To solve this problem, Zhu et al. [29] incorporated a prescribed error constraint approach with BC to bind the spacing error within the desired value range to prevent error propagation. Adaptive laws were used to approximate uncertain vehicle parameters. Kwon and Chwa [30] proposed an adaptive coupled sliding mode control (SMC) for a BD communication scheme, and adaptive laws were used to estimate the unknown, uncertain second-order ND. Zuo et al. [31] developed a distributed adaptive integral SMC (ISMC) for a platoon with QSP. Feedback linearization was applied to linearize the ND by assuming known dynamics expression as in Ref. [32]. Yan et al. [33] presented an adaptive neural SMC for a BD platoon by integrating velocity and input saturation into the control design. The uncertain term was approximated by radial basis function neural network (RBF-NN). Guo et al. [34] proposed a fault-tolerant ISMC with unknown and linear actuator dead-zone quantization for the BD IFTs. The study used a third-order ND with quantization and a modified constant-time headway policy (MCTHP). Moreover, they implemented a minimum parameter learning RBF-NN (MPL-RBF-NN) to approximate the unknown external term. Such MPL-RBF-NN technique minimizes the number of adaptive parameters to only one by using the norm of the neural weight vector. Similar approaches were also reported with a new QSP and improved QSP that accounts for actuator fault in the spacing policy [35]. Guo et al. [36] also proposed prescribed performance control (PPC) with SMC for the PLF and the BDL IFTs considering actuator saturation. To include the leader vehicle's information and for simplicity, they considered a CDGP so that it is convenient to define a lumped spacing error term. By defining similar error-constraining functions for all vehicles, SS of the platoon was achieved. A similar approach has also been proposed in Ref. [37].

In previous studies, linearized vehicle models were accustomed to easing the difficulty of finding the Laplace transform of the spacing error terms for nonlinear vehicle models to guarantee the SS of the platoon [38]. In some other studies, an SMC was also proposed for nonlinear systems under the bidirectional IFT, in which case it was possible to get the Laplace transform for the error terms [39]. However, these assumptions ignore the physical system's complexity and most IFT options. Inter-vehicle spacing highly depends on weather, road conditions, visibility, braking performance, etc. In previous studies, the SP mainly do not address road demands and achieve traffic stability. Moreover, the existing estimation laws for unknown terms, such as adaptive laws, type-1 fuzzy systems, and neural approximation techniques, have some drawbacks. In the adaptive estimation approach, an explicit adaptive law is required to approximate each unknown term, and this would result in additional instability and computational burden. Conversely, the type-1 fuzzy systems and neural networks employed in control are mostly based upon an assumption of a deterministic mean and standard deviations for the membership functions (MFs). We have consolidated the abovementioned studies in Table 1.

Building upon the insights from previous studies, this paper presents a prescribed performance backstepping and sliding mode control (BSMC), and the key contributions are outlined as follows:

(1) We introduce an asymmetric prescribed time transformation function to limit spacing errors between vehicles. This approach ensures not only string stability but also constrains the spacing error within predefined bounds and a specified settling time.
(2) To address uncertainties in the input values and approximate unknown nonlinear terms, we design an adaptive interval type-2 fuzzy logic system (IT2FLS). This approach yields interval outputs, incorporating uncertain mean and standard deviation in the membership functions of inputs, thereby enhancing the system's adaptability.
(3) We propose an exponential spacing policy (ESP) to incorporate environmental factors and vehicle constraints through adaptable safety parameters. Unlike CTGP and QSP, ESP fosters a stable traffic flow by meticulously tuning these parameters to the driving context.
(4) Our control strategy combines BC and SMC techniques. We incorporate BC due to its seamless integration capabilities with various control schemes and SMC to enhance system adaptability and robustness, offering a chattering-free reaching law. Furthermore, we introduce additive and multiplicative fault types in our control design to ensure practical relevance, compensating for real-world performance degradation scenarios. This amalgamation of methodologies offers enhanced stability, adaptability, and robustness in automated vehicular systems control.

The remainder of the article is structured as follows: Sec. 2 provides an overview of the preliminaries and the problem formulation. Section 3 explores the theory behind IT2FLS. Section 4 covers the control system's design and the platoon system's stability analysis. Section 5 offers a simulation example to demonstrate the effectiveness of the proposed control strategy, while Sec. 6 concludes the article with final remarks.

Table 1 Summary of existing research in the literature and this study

Ref.	ND	Method	IFT	SP	Approximation	SS
[12]	Second-order nonlinear	Coupled SMC	PF	SSP	–	Yes
[27]	Third-order nonlinear	BC	PF	CDGP	Cerebellar NN	No
[28]	Third-order nonlinear	BC	PF	CTGP	–	No
[29]	Third-order nonlinear	BC	PF	CTGP	Adaptive	Yes
[30]	Second-order nonlinear	Coupled SMC	BD	CDGP	Adaptive	Yes
[31]	Third-order nonlinear	Coupled SMC	BD	QSP	RBF-NN	Yes
[33]	Second-order nonlinear	Adaptive SMC	BD	CDGP	RBF-NN	Yes
[34]	Third-order nonlinear	Coupled SMC	BD	MCTHP	MPL-RBF-NN	Yes
[35]	Third-order nonlinear	Coupled SMC	BD	Improved QSP	MPL-RBF-NN	Yes
[36]	Third-order nonlinear	Coupled SMC	BD	Improved fault-QSP	MPL-RBF-NN	Yes
[37]	Second-order nonlinear	Coupled PPC-SMC	BD	Improved QSP	MPL-RBF-NN	Yes
[40]	Third-order nonlinear	BC	PF	CTGP	Type-1 FLS	Yes
This study	Third-order nonlinear	PPC-BSMC	PF	ESP	IT2FLS	Yes

2 Preliminaries and Problem Formulation

2.1 Preliminaries

*2.1.1 **Notation**.* $|\cdot|$ denotes the absolute value of a number, $\|\cdot\|$ represents the Euclidean norm of a vector, $\|\cdot\|_\infty$ is also an infinity norm, $\mathbb{R}^n$ is the space for the real numbers of n dimensions, $\mathbb{R}^+$ represents positive real numbers, $\sup(\cdot)$ denotes the least upper bound from the set, $\min(\cdot)$ represent a value to which the functional value is less than or equal to the local minimum or absolute minimum value, $\operatorname{argmin}_\Delta$ denotes the point or element of the domain of a function to be minimized, **sign** represents the sigmoid function to show the property of a real number of being either positive, negative, or zero.

LEMMA 1 ([41]). *Let $\Omega(\mathbf{x})$ be a Lipschitz-continuous function defined on a compact set Δ_c. For an upper bound of the approximation error $\varepsilon_{\max}$, there exist a fuzzy logic system (FLS) approximator $\hat{\boldsymbol{\theta}}^T\boldsymbol{\zeta}(\mathbf{x})$ such that*

$$\sup_{\mathbf{x}\in\Delta_c}\left\|\hat{\boldsymbol{\theta}}^T\zeta(\mathbf{x})-\Omega(\mathbf{x})\right\|\le\varepsilon_{\max} \tag{1}$$

where $\mathbf{x}$ is the FLS input vector, and $\hat{\boldsymbol{\theta}}=[y^1,y^2,\ldots,y^M]^T\in\mathbb{R}^M$ is the parameter vector. The basis function vector $\zeta(\mathbf{x})$ will be defined in the next section. The optimal parameter vector θ^* can be given as

$$\boldsymbol{\theta}^*=\underset{\theta\in\mathbb{R}^n}{\operatorname{argmin}}\left[\sup_{\mathbf{x}\in\Delta_c}\left\|\hat{\boldsymbol{\theta}}^T\zeta(\mathbf{x})-\Omega(\mathbf{x})\right\|\right] \tag{2}$$

Thus, the function $\Omega(\mathbf{x})$ can be represented as

$$\Omega(\mathbf{x})=\theta^{*T}\zeta(\mathbf{x})+\varepsilon(\mathbf{x}) \tag{3}$$

LEMMA 2 ([42]). *Let $V(t)\in[0,\infty)$, $\forall\, t\in R^+$, be a smooth positive definite function regarding the states. And suppose that*

$$\dot{V}(t)\le-\Upsilon V(t)+\Gamma\quad\forall\, t\ge t_0\ge 0 \tag{4}$$

For a finite value $\Upsilon>0$ and $\Gamma>0$, we can imply that

$$V(t)\le e^{-\Upsilon(t-t_0)}V(t_0)+\int_{t_0}^{t}e^{-\Upsilon(t-\tau)}\Gamma(\tau)\,\mathrm{d}\tau \tag{5}$$

2.2 Vehicle Dynamics Modeling. This study explores a scenario involving a group of N automated vehicles connected via PF IFT following a leader vehicle driven by a human, as shown in Fig. 1. The PF communication scheme is the simplest, where a vehicle receives information only from its immediate predecessor. The rest of the IFTs require a complex information exchange strategy requiring long-range sensing technology and smart infrastructures.

The uncertain nonlinear longitudinal dynamics of vehicle i can be expressed as

$$\begin{aligned}\dot{p}_i(t)&=v_i(t)\\ \dot{v}_i(t)&=a_i(t)\\ \dot{a}_i(t)&=\Lambda_i(t)+G_iu_i(t)+d_i(t)\end{aligned} \tag{6}$$

where $p_i(t)$, $v_i(t)$, and $a_i(t)$ are the position, velocity, and acceleration of vehicle i, respectively. $u_i(t)\in\mathbb{R}^1$ is the control input to vehicle i's engine, $G_i=1/m_i\tau_i$ is the coefficient of the control input, m_i is the vehicle mass, τ_i is the engine time lag, $d_i(t)$ is an unknown bounded exogenous disturbance where $|d_i(t)|\le d_{\max,i}$, $\Lambda_i(t)$ is an unknown nonlinear term given as

$$\begin{aligned}\Lambda_i(t)=&-\frac{1}{\tau_i}\left[a_i(t)+\frac{1}{2m_i}\rho' C_{d,i}A_{f,i}v_i(t)^2+\frac{d_{m,i}}{m_i}\right]\\&-\frac{1}{m_i}\rho' C_{d,i}A_{f,i}v_i(t)a_i(t)\end{aligned} \tag{7}$$

where ρ' is the air density, $C_{d,i}$ is the aerodynamic drag coefficient, $C_{r,i}$ is the rolling resistance coefficient, $A_{f,i}$ is the frontal cross-sectional area of vehicle i, m_i is the mass of vehicle i, $d_{m,i}$ is the mechanical drag on vehicle i, and τ_i is the driving system lag time of vehicle i. The detailed derivation of Eq. (7) can be found in Appendix A. In practical scenarios, actuators experience failures resulting from wear and aging of components. These failures lead to response delays and introduce dead zones during control. Considering that the vehicle is subjected to unknown actuator faults, we re-write the expression for $u_i(t)$. In this paper, a multiplicative and additive fault was considered. Loss of actuator effectiveness can be measured with $\eta_i(t)\in(0,1]$. The actual control input $u_i(t)$ in Eq. (6) can be written as

$$u_i(t)=\eta_i(t)\hat{u}_i(t)+u_{f,i}(t),\quad t>t_f \tag{8}$$

where $u_{f,i}(t)$ is the unknown additive fault, t_f is the time at which the actuator fails, $\eta_i(t)=0$ shows the complete failure of the actuator, and $\eta_i(t)=1$ indicates full functionality of the actuator; therefore, we have $0\le\eta_{i,\min}\le\eta_i(t)\le\eta_{i,\max}$ where $\eta_{i,\min}$ and $\eta_{i,\max}$ are known constants. $\hat{u}_i(t)$ is the new control input to be designed. Substituting Eq. (8) into Eq. (6), we can get

$$\dot{p}_i(t)=v_i(t) \tag{9}$$

$$\dot{v}_i(t)=a_i(t) \tag{10}$$

$$\dot{a}_i(t)=\Omega_i(t)+G_i\eta_i(t)\hat{u}_i(t) \tag{11}$$

where $\Omega_i(t)=\Lambda_i(t)+G_iu_{f,i}(t)+d_i(t)$ is the unknown nonlinear term which cannot be obtained in reality, and will be approximated by a fuzzy approximation system as in Eq. (3). This paper proposes utilizing an IT2FLS to approximate the unknown term. The details of this approach will be elaborated upon in Sec. 3.

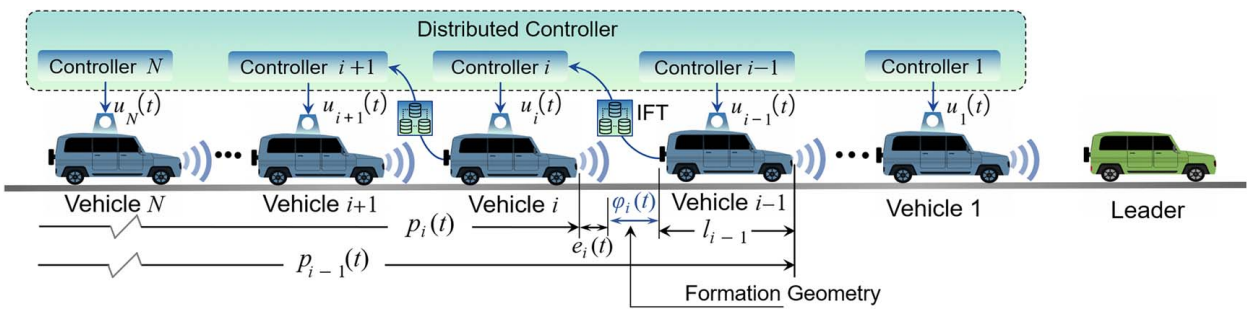

Fig. 1 Connected and automated platoon

2.3 Prescribed Tracking Performance. Define the spacing error of vehicle i as

$$e_i(t) = p_{i-1}(t) - p_i(t) - l_{i-1} - \varphi_i(t) \tag{12}$$

where l_{i-1} is the preceding vehicle's length, and $\varphi_i(t)$ is the desired inter-vehicle spacing. The proposed desired spacing is called the ESP policy, which addresses pertinent factors essential for the autonomous driving system, encompassing acceleration limits, road conditions, and environmental considerations. It is formulated as follows:

$$\varphi_i(t) = d_{o,i} + \vartheta_i \frac{v_i(t)^2}{2a_{\max,i}} + \kappa_{1,i}\left(1 - \exp\left(-\frac{v_i(t)}{\kappa_{2,i}}\right)\right) \tag{13}$$

where $d_{o,i}$ is the standstill spacing, $a_{\max,i}$ is the maximum vehicle deceleration, ϑ_i is the safety coefficient based on road and weather conditions, and $\kappa_{1,i}$ and $\kappa_{2,i}$ are the design parameters [14]. $\psi_{\min}$ is the minimum traffic density, $\psi_{\max}$ is the maximum traffic density, and ψ_{cr} is the critical density where there is a transition of the stability and instability occurs. $Q(\cdot)$ is the traffic flowrate.

$$\begin{aligned} &\psi_{\min} \le \psi_{cr} \le \psi_{\max} \\ &Q(\psi_{\min}) = Q(\psi_{\max}) = 0 \\ &\left.\frac{\partial Q}{\partial \rho}\right|_{\psi=\psi_{cr}} = 0 \end{aligned} \tag{14}$$

The traffic flowrate $Q(\psi(v_i(t)))$ can be computed as

$$Q\big(\psi(v(t))\big) = \frac{v(t)}{d_o + \vartheta \dfrac{v(t)^2}{2a_{\max}} + \kappa_1\left(1 - \exp\left(\dfrac{-v(t)}{\kappa_2}\right)\right)} \tag{15}$$

As $Q(\psi(v(t)))$ is continuous in an interval $[\psi_{\min}, \psi_{\max}]$ and differentiable over an open interval $(\psi_{\min}, \psi_{\max})$, and $Q(\psi_{\min}) = Q(\psi_{\max})$ (i.e., Eq. (14) holds), based on Rolle's theorem (see Appendix B), there exists at least one point $\psi_{cr} \in (\psi_{\min}, \psi_{\max})$ such that $\partial Q(\psi = \psi_{cr})/\partial\psi = 0$. For string stable operation, the parameters κ_1 and κ_2 should satisfy the inequality:

$$\ln\left(\frac{\vartheta a_{\max}}{\vartheta \kappa_2^2}\right) \ge \frac{2\tau a_{\max}}{\vartheta \kappa_2} - 1 \tag{16}$$

where τ is the time lag of the driving system.

On the other hand, a CTGP consistently leads to an unstable traffic flow at all traffic densities as $\partial Q/\partial\psi = -d_o/v(t)$ is negative. We can prove the same for the human-like spacing policy named QSP [14].

Moreover, the paper aims to bind the spacing error in a prescribed error range using a fixed-time prescribed transformation performance function so that the following inequality holds:

$$-\rho_{s,i}\delta_{\min,i} < e_i(t) < \rho_{s,i}\delta_{\max} \tag{17}$$

where $\rho_{s,i}$ is the minimum steady-state error near zero, and $\delta_{\min,i}$ and $\delta_{\max}$ are the minimum and maximum value of the asymmetric error constraint constants, respectively. Hence, the error $e_i(t)$ would converge to an asymmetric error bound region near zero: $O_{e_i} := (-\rho_{s,i}\delta_{\min,i},\ \rho_{s,i}\delta_{\max})$.

2.4 Control Objectives. This paper aims to develop an adaptive backstepping and sliding mode platoon control strategy capable of handling actuator faults, unknown external forces, and disturbances while meeting the following stringent requirements:

(1) Individual vehicle stability [10]: Each follower vehicle tracks the leader's trajectory with bounded spacing errors in fixed time.
(2) A prescribed performance for the tracking error is achieved by the vehicles in the platoon, ensuring that the tracking error is strictly steered into a predefined region bounded by a fixed-time prescribed transformation performance function.
(3) SS of the automated platoon is guaranteed under either of the following conditions:

DEFINITION 1 (SS [10]). *The tracking errors $e_i(t)$ of the vehicles with dynamics in (6) are said to be string stable for any $e_{\max,i}$; there exists $\nu > 0$ such that*

$$\|e_i(0)\|_\infty < \nu \Rightarrow \sup\|e_i(t)\|_\infty < e_{\max,i} \quad \text{for } i \in N$$

DEFINITION 2 (Strong SS [30,43]). *The tracking error of each vehicle in the platoon system is said to be string stable if $|e_1(t)| \ge |e_2(t)| \cdots \ge |e_{N-1}(t)| \ge |e_N(t)|$. This also means that the spacing error should not propagate along the tail of the vehicle string.*

3 Interval Type-2 Fuzzy Logic System

A fuzzy logic system consists of rules where knowledge-based terms, also named antecedents, are used to define the inputs as MFs to reach arguments, also known as consequents. As the knowledge to construct the rules is usually uncertain, the membership functions in the antecedent and consequent parts must also be uncertain. Type-1 fuzzy systems are those whose MFs are type-1 fuzzy sets (T1FS) in which we have exact mean and standard deviation values. IT2FLS is a fuzzy system that uses one or more interval type-2 fuzzy sets (IT2FS) in the antecedent or consequence part of its rule base. The difference between the type-1 and the type-2 fuzzy systems is the introduction of uncertainties in their MF. The output of IT2FLS is an interval rather than a crisp value, as in type-1 FLS. Therefore, type reduction (TR) methods must be employed to reduce the IT2FS into T1FS [44–46]. Figure 2(*a*) shows the general framework of IT2FLS. The specific procedure of each layer is discussed as follows.

3.1 Input Layer. In this layer, we have n number of inputs. Consider the input to the fuzzy system $\mathbf{x} = [x_k]^T = [x_1, x_2, \ldots, x_n]^T$ (for $k = 1, 2, \ldots, n$).

3.2 Fuzzification/Membership Layer. Consider a Gaussian membership function with a fixed mean value and an uncertain standard deviation given as follows:

$$\mu_{\tilde{A}_k^{s_k}} = \exp\left[-\frac{1}{2}\left(\frac{x_k - \hat{m}_k^{s_k}}{\sigma_k^{s_k}}\right)^2\right] \tag{18}$$

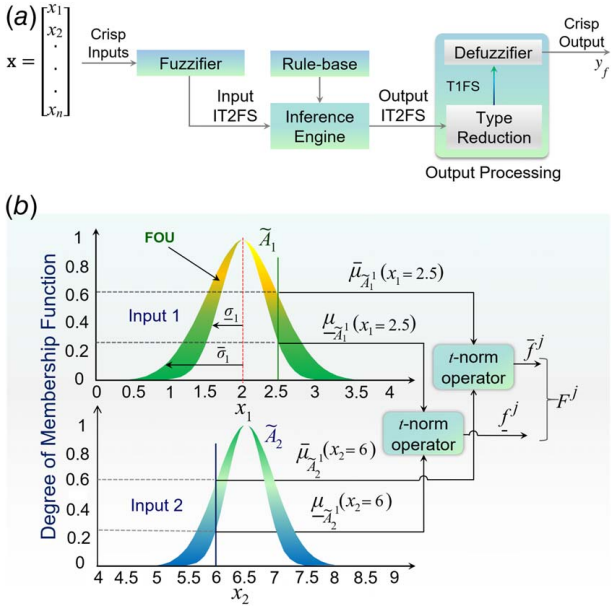

Fig. 2 Interval type-2 fuzzy logic system: (*a*) general framework of IT2FLS and (*b*) *t*-norm operation for two-input case

where $\mu_{\tilde{A}_k^{s_k}}$ is s_k^{th} MF for the kth input, $\hat{m}_k^{s_k}$ is the mean/center of the s_k^{th} MF for kth input, and $\sigma_k^{s_k}$ is the standard deviation of the s_k^{th} MF for kth input. We consider $h_k = h$ number of MFs and $s_k = 1, 2, \ldots, h$. The output of each MF can be represented by an interval $[\underline{\mu}_{\tilde{A}_k^{s_k}}, \overline{\mu}_{\tilde{A}_k^{s_k}}]$ to represent the lower and upper MF represented as

$$\underline{\mu}_{\tilde{A}_k^{s_k}} = \exp\left[-\frac{1}{2}\left(\frac{x_k - \hat{m}_k^{s_k}}{\underline{\sigma}_k^{s_k}}\right)^2\right]$$
$$\overline{\mu}_{\tilde{A}_k^{s_k}} = \exp\left[-\frac{1}{2}\left(\frac{x_k - \hat{m}_k^{s_k}}{\overline{\sigma}_k^{s_k}}\right)^2\right] \tag{19}$$

where $\underline{\mu}_{\tilde{A}_k^{s_k}}$ and $\overline{\mu}_{\tilde{A}_k^{s_k}}$ are the lower and upper membership degrees for the inputs.

3.3 Rule-Base Layer. The interval type-2 fuzzy rule base contains a collection of IF-THEN rules. In this layer, we have a total number of $M = \prod_k^n h_k = h^n$ fuzzy rules. Based on the Mamdani fuzzy inference system, the jth fuzzy rule R^j of the fuzzy system is expressed as

$$R^j: \text{IF} \quad x_1 \text{ is } \tilde{A}_1^j \text{ and}: \cdots \text{ and } x_n \text{ is } \tilde{A}_n^j \text{ THEN } y_f \text{ is } B^j$$

where R^j(for $j = 1, 2, \ldots, M$) are the fuzzy rules, $\tilde{A}_k^j$ is antecedent IT2FS of kth input, B^j is consequent/output IT2FS, and y_f is the crisp output of the IT2FLS.

3.4 Inference Engine. This layer performs a combination of M fuzzy rules, maps the input's IT2FS into output interval type-2 sets using t-norm operation, and performs the intersection of the antecedent FS. The uncertainty in the primary membership function forms a shaded area called the footprint of uncertainty. Figure 2(*b*) illustrates the t-norm operation for a two-input case, each having one MF.

Using a product t-norm operator, we compute the upper and lower firing strength of the jth rule, i.e., $F^j = [\underline{f}^j, \overline{f}^j]$.

$$\underline{f}^j = \prod_{k=1}^{n} \underline{\mu}_{\tilde{A}_k^j}(x_k), \quad \overline{f}^j = \prod_{k=1}^{n} \overline{\mu}_{\tilde{A}_k^j}(x_k) \tag{20}$$

where $\underline{f}^j$ and $\overline{f}^j$ are the left-most and right-most points of F^j, respectively. Moreover, the index j corresponds to the multiplication of the indexes of the antecedent sets.

3.5 Type-Reduction Layer. In this layer, we generate an interval T1FS. To reduce the IT2FS to T1FS, we used the closed-form Nie-Tan TR method [47].

Normalizing the firing strengths will give a fuzzy basis vector $\zeta(\mathbf{x}) = [\zeta_l^T(\mathbf{x}), \zeta_r^T(\mathbf{x})]^T$. The left and right basis terms are defined as

$$\zeta_l(\mathbf{x}) = \frac{\underline{f}^j}{\sum_{j=1}^{M} \underline{f}^j}, \quad \zeta_r(\mathbf{x}) = \frac{\overline{f}^j}{\sum_{j=1}^{M} \overline{f}^j} \tag{21}$$

Based on the Nie-Tan TR method, we have

$$\zeta(\mathbf{x}) = \frac{\underline{f}^j + \overline{f}^j}{\sum_{j=1}^{M}\left(\underline{f}^j + \overline{f}^j\right)} \tag{22}$$

3.6 Defuzzification Layer. Let $y^j \in \mathbb{R}$ be a free parameter representing all points that maximize the MF of the output, i.e., $\mu_{B_n^j}$ and put into the set $\hat{\boldsymbol{\theta}} \in \mathbb{R}^M$. Hence, the expression for the approximated term $\hat{\Omega}(\mathbf{x}|\hat{\theta})$ will be given as

$$y_f = \hat{\Omega}(\mathbf{x}|\hat{\theta}) = \hat{\boldsymbol{\theta}}^T \boldsymbol{\zeta}(\mathbf{x}) \tag{23}$$

where $\hat{\boldsymbol{\theta}} = [y^1, y^2, \cdots, y^M]^T$ is the parametric vector.

4 Controller Design and Stability Analysis

4.1 Controller Design. In this section, we design a prescribed performance hybrid BSMC. We now integrate a prescribed performance control with the main controller to constrain the tracking error defined in Eq. (12) to achieve a desired prescribed error range as in Eq. (17). The framework for the proposed control is illustrated in Fig. 3. Inspired by Refs. [48,49], we choose a transformation performance function as

$$\rho_i(t) = \begin{cases} \dfrac{t_s^4 w(t)}{(1-\rho_{s,i})(t_s - t)^4 + \rho_{s,i} t_s^4 w(t)}, & 0 \le t < t_s \\ \dfrac{1}{\rho_{s,i}}, & t \ge t_s \end{cases} \tag{24}$$

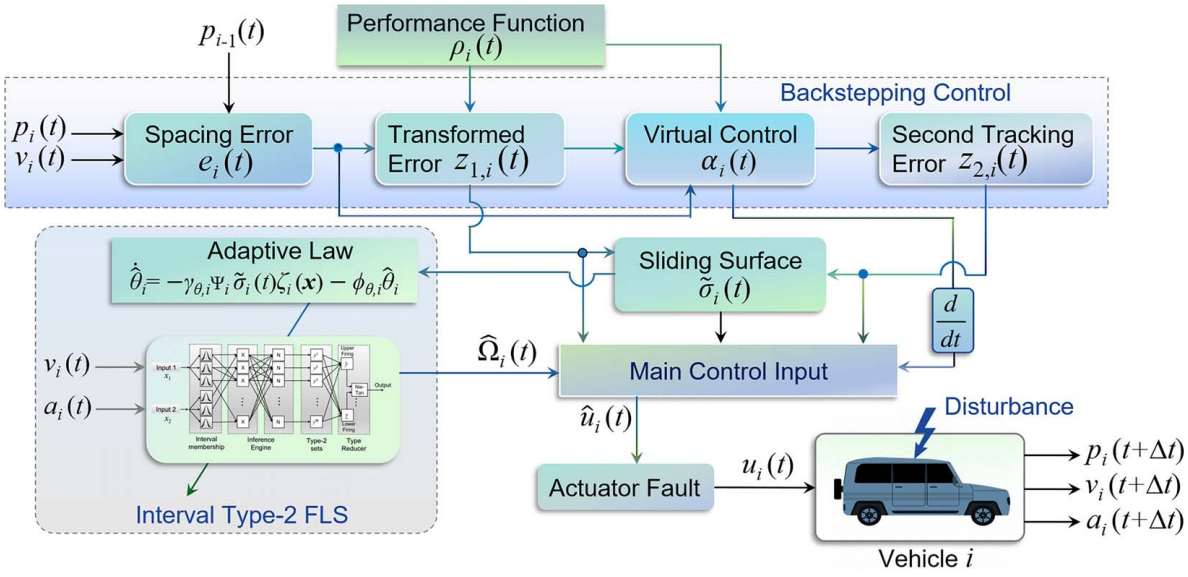

Fig. 3 Proposed control framework

where t_s denotes the preset finite settling time, $0 \le \rho_{s,i} \le 1$ is the desired minimum steady-state error, $w(t)$ represent a strictly increasing and smooth function, and $w(0) = 1$.

LEMMA 3 ([50]). *The transformation performance function $\rho_i(t)$ be defined as in (24) and hence the following three properties hold:*

(1) *For $t \in [0, t_s)$, the function $\rho_i(t)$ with $\rho_i(0) = 1$ is a strictly increasing function and the final value reaches $1/\rho_{s,i}$ at $t = t_s$ and remains the constant for $t \in [t_s, \infty]$.*
(2) *$\dot{\rho}_i$ and $\ddot{\rho}_i$ are continuously differentiable and bounded $\forall t \ge 0$; $\rho^{(3)}$ is continuous and bounded everywhere.*
(3) *The term $\hat{\delta}_i = \rho_i^{-1}\dot{\rho}_i$ have continuous derivatives and bounded functions, and $\dot{\hat{\delta}}$ is also continuous and bounded everywhere.*

The proposed control strategy must ensure that each vehicle's spacing error converges and steers into a predetermined threshold within a specified settling time and speed. Hence, we define a transformed error term as

$$\xi_i(t) = \rho_i(t)e_i(t), \qquad i = 1, 2, \ldots, N \tag{25}$$

$$z_{1,i}(t) = \lambda_i \xi_i(t), \quad z_{2,i}(t) = \dot{e}_i(t) - \alpha_i(t) \tag{26}$$

with

$$\lambda_i(t) = \frac{1}{(\delta_{\max,i} - \xi_i(t))(\delta_{\min,i} + \xi_i(t))}$$

where $z_{1,i}(t)$ *is the transformed position tracking error*, $z_{2,i}(t)$ *is the second tracking error which will be defined later, and* $\alpha_i(t)$ *is the virtual control input which will be designed later.*

For an asymmetric error constraint, it is noticeable that $z_{1,i}(t)$ is applicable in the compact set $O_\xi := \{-\delta_{\min,i} < \xi_{1,i}(t) < \delta_{\max,i}\}$ and for any $-\delta_{\min,i} < \xi_{1,i}(0) = e_{1,i}(0) < \delta_{\max,i}$, if $z_{1,i}(t)$ is bounded for all $t \ge 0$, it will inherently be assured that $\xi_i(t) \in O_\xi$ for all $t \ge 0$. For all the vehicles $(i = 1, 2, \ldots, N)$, $e(t) = \rho^{-1}(t)\xi(t)$ and bounded $\xi(t)$, we therefore can achieve $e(t)$ to be bounded in the prescribed asymmetric boundary as

$$\begin{cases} -(1-\rho_s)\left(\dfrac{t_s - t}{t_s}\right)^4 w^{-1}(t)\delta_{\min} - \rho_s\delta_{\min} \le e(t) < \\ \qquad (1-\rho_{s,i})\left(\dfrac{t_s - t}{t_s}\right)^4 w^{-1}(t)\delta_{\max} + \rho_s\delta_{\max}, & 0 \le t < t_s \\ -\rho_s\delta_{\min} < e(t) < \rho_s\delta_{\max}, & t \ge t_s \end{cases} \tag{27}$$

Remark 1. In the proposed control approach, an asymmetric bound can be defined for a more general case where $\delta_{\min} \ne \delta_{\max}$. Moreover, we only need a rough estimation of the initial error to design $\delta_{\min}$ and $\delta_{\max}$ to satisfy $-\delta_{\min,i} < e_{1,i}(0) < \delta_{\max,i}$ $(i = 1, 2, \ldots, N)$, unlike some control techniques that demand a precise initial value. If we define larger upper and lower bounds, we can control the error by defining the desired steady-state error value ρ_s. ∎

Thus, the time derivative of $\xi_i(t)$ can be obtained as

$$\begin{aligned} \dot{\xi}_i(t) &= \dot{\rho}_i(t)e_i(t) + \rho_i(t)\dot{e}_i(t) \\ &= \dot{\rho}_i(t)e_i(t) + \rho_i(t)\big(z_{2,i}(t) + \alpha_i(t)\big) \end{aligned} \tag{28}$$

Computing the time derivative of $z_{1,i}(t)$ and substituting the expression of $\dot{\xi}_i(t)$ into it yields

$$\begin{aligned} \dot{z}_{1,i}(t) &= \varrho_i\dot{\xi}_i(t) \\ &= \varrho_i\rho_i(t)\big(\rho_i^{-1}\dot{\rho}_i(t)e_i(t) + z_{2,i}(t) + \alpha_i(t)\big) \end{aligned} \tag{29}$$

where

$$\varrho_i = \frac{\delta_{\max,i}\delta_{\min,i} + \xi_i^2}{(\delta_{\max,i} - \xi_i(t))^2(\delta_{\min,i} + \xi_i(t))^2}$$

Construct the candidate Lyapunov function as

$$V_{1,i}(t) = \frac{1}{2}z_{1,i}^2(t) \tag{30}$$

The time derivative of $V_{1,i}(t)$ gives

$$\dot{V}_{1,i}(t) = z_{1,i}(t)\varrho_i\rho_i(t)\big(\rho_i^{-1}(t)\dot{\rho}_i(t)e_i(t) + z_{2,i}(t) + \alpha_i(t)\big) \tag{31}$$

Design the virtual control input as

$$\alpha_i(e_i, \hat{\delta}_i, t) = -\frac{c_{1,i}\lambda_i(t)e_i(t)}{\varrho_i} - \rho_i^{-1}(t)\dot{\rho}_i(t)e_i(t) \tag{32}$$

where $c_{1,i}$ is a positive design constant. Substituting (32) into (31) yields

$$\begin{aligned} \dot{V}_{1,i}(t) &= -c_{1,i}\lambda_i(t)\rho_i(t)e_i(t)z_{1,i}(t) + \varrho_i\rho_i(t)z_{1,i}(t)z_{2,i}(t) \\ &= -c_{1,i}z_{1,i}^2(t) + \varrho_i\rho_i(t)z_{1,i}(t)z_{2,i}(t) \end{aligned} \tag{33}$$

For perfect tracking, $z_{2,i}(t)$ should be 0, so that we will have $\dot{V}_{1,i}(t) \le 0$. We define the second tracking error $z_{2,i}(t)$ as

$$\begin{aligned} z_{2,i}(t) = v_{i-1}(t) - v_i(t) - \frac{\vartheta_i}{a_{\max,i}}v_i(t)a_i(t) \\ - \frac{\kappa_{1,i}}{\kappa_{2,i}}\exp\left(-\frac{v_i(t)}{\kappa_{2,i}}\right)a_i(t) - \alpha_i(\cdot) \end{aligned} \tag{34}$$

The derivative of $z_{2,i}(t)$ in (34) with respect to time gives

$$\dot{z}_{2,i}(t) = a_{i-1}(t) - a_i(t) - \omega_i a_i^2(t) - \Psi_i\dot{a}_i(t) - \dot{\alpha}_i(\cdot) \tag{35}$$

where

$$\omega_i = \frac{\vartheta_i}{a_{\max,i}} - \frac{\kappa_{1,i}}{\kappa_{2,i}^2}\exp\left(-\frac{v_i(t)}{\kappa_{2,i}}\right)$$

$$\Psi_i = \frac{\vartheta_i}{a_{\max,i}}v_i(t) + \frac{\kappa_{1,i}}{\kappa_{2,i}}\exp\left(-\frac{v_i(t)}{\kappa_{2,i}}\right) > 0$$

Now, let us introduce SMC control to the backstepping control design. Define a sliding surface $\tilde{\sigma}_i(t)$ as

$$\tilde{\sigma}_i(t) = z_{2,i}(t) + c_{2,i}z_{1,i}(t) \tag{36}$$

where $c_{2,i}$ is a positive design constant. The derivative of Eq. (36) with respect to time yields

$$\dot{\tilde{\sigma}}_i(t) = \dot{z}_{2,i}(t) + c_{2,i}\dot{z}_{1,i}(t) \tag{37}$$

Plugging Eq. (32) into Eq. (29) gives the expression for $\dot{z}_{1,i}(t)$ as

$$\dot{z}_{1,i}(t) = -c_{1,i}z_{1,i}(t) + \varrho_i\rho_i(t)z_{2,i}(t) \tag{38}$$

Substituting Eqs. (35) and (38) into Eq. (37) will give

$$\begin{aligned} \dot{\tilde{\sigma}}_i(t) = a_{i-1}(t) - a_i(t) - \omega_i a_i^2(t) - \Psi_i\dot{a}_i(t) - \dot{\alpha}_i(\cdot) \\ + c_{2,i}\big(-c_{1,i}z_{1,i}(t) + \varrho_i\rho_i(t)z_{2,i}(t)\big) \end{aligned} \tag{39}$$

The derivative term of the virtual control $\dot{\alpha}_i(e_i, \hat{\delta}_i, t)$ can be computed as

$$\begin{aligned} \dot{\alpha}_i(\cdot) = e_i(t)\dot{\hat{\delta}}_i - \dot{e}_i(t)\hat{\delta}_i + c_{1,i}e_i(t)\dot{\xi}_i(t)\frac{\delta_{\min} + \xi_i(t)}{\xi_i^2(t) + \delta_{\min}\delta_{\max}} \\ - c_{1,i}\dot{e}_i(t)\frac{(\delta_{\min} + \xi_i(t))(\delta_{\max} - \xi_i(t))}{\xi_i^2(t) + \delta_{\min}\delta_{\max}} \\ - c_{1,i}e_i(t)\dot{\xi}_i(t)\frac{\delta_{\max} - \xi_i(t)}{\xi_i^2(t) + \delta_{\min}\delta_{\max}} \\ + 2c_{1,i}e_i(t)\xi_i(t)\dot{\xi}_i(t)\frac{(\delta_{\min} + \xi_i(t))(\delta_{\max} - \xi_i(t))}{(\xi_i^2(t) + \delta_{\min}\delta_{\max})^2} \end{aligned} \tag{40}$$

with

$$\hat{\delta}_i = \frac{\dot{\rho}_i(t)}{\rho_i(t)} = \begin{cases} \dfrac{(1-\rho_{s,i})(t_s-t)^3[(t_s-t)\dot{w}(t)+4w(t)]}{w(t)\left[(1-\rho_{s,i})(t_s-t)^4+\rho_{s,i}t_s^4 w(t)\right]}, & t < t_s \\ 0, & t \geq t_s \end{cases} \tag{41}$$

$$\dot{\hat{\delta}}_i = \frac{\ddot{\rho}_i(t)}{\rho_i(t)} - \frac{\dot{\rho}_i(t)^2}{\rho_i^2(t)} = \begin{cases} \dfrac{\dot{b}q - b\dot{q}}{q^2}, & t < t_s \\ 0, & t \geq t_s \end{cases} \tag{42}$$

And

$$\begin{aligned} b &= (1-\rho_{s,i})(t_s-t)^3[(t_s-t)\dot{w}(t)+4w(t)] \\ \dot{b} &= -3(1-\rho_{s,i})(t_s-t)^2[(t_s-t)\dot{w}(t)+4w(t)] \\ &\quad + (1-\rho_{s,i})(t_s-t)^3[(t_s-t)\ddot{w}(t)+3\dot{w}(t)] \\ q &= (1-\rho_{s,i})(t_s-t)^4 w(t) + \rho_{s,i}t_s^4 w^2(t) \\ \dot{q} &= (1-\rho_{s,i})(t_s-t)^4\dot{w}(t) - 4(1-\rho_{s,i})(t_s-t)^3 w(t) + 2\rho_{s,i}t_s^4\dot{w}(t)w(t) \end{aligned}$$

Referring (3), Eq. (11) can be re-written as

$$\dot{a}_i(t) = \theta_i^{*T}\zeta_i(\mathbf{x}) + \varepsilon_i(t) + G_i\eta_i(t)\hat{u}_i(t) \tag{43}$$

Substituting Eq. (43) into Eq. (39), one can obtain

$$\begin{aligned} \dot{\tilde{\sigma}}_i(t) = a_{i-1}(t) - a_i(t) - \omega_i a_i^2(t) - \Psi_i\big(\theta_i^{*T}\zeta_i(\mathbf{x}) + \varepsilon_i(t) \\ + G_i\eta_i(t)\hat{u}_i(t)\big) - \dot{\alpha}_i(\cdot) + c_{2,i}\big(-c_{1,i}z_{1,i}(t) + \varrho_i\rho_i z_{2,i}(t)\big) \end{aligned} \tag{44}$$

Based on the inequality defined in Sec. 2, we have the following inequality as in Ref. [51], i.e.,

$$\eta_i(t)\hat{u}_i(t) \geq \eta_{\min,i}\hat{u}_i(t) \tag{45}$$

Multiplying (39) with $\tilde{\sigma}_i(t)$ gives

$$\begin{aligned} \tilde{\sigma}_i(t)\dot{\tilde{\sigma}}_i(t) &= \tilde{\sigma}_i(t)\big(a_{i-1}(t) - a_i(t) - \omega_i a_i^2(t) - \dot{\alpha}_i(\cdot) \\ &\quad -\Psi_i\theta_i^{*T}\zeta_i(\mathbf{x})\big) - \Psi_i\tilde{\sigma}_i(t)\varepsilon_i(t) - G_i\tilde{\sigma}_i(t)\eta_i(t)\hat{u}_i(t) \\ &\quad + \tilde{\sigma}_i(t)c_{2,i}\big(-c_{1,i}z_{1,i} + \varrho_i\rho_i z_{2,i}\big) \\ &\leq \tilde{\sigma}_i(t)\big(a_{i-1}(t) - a_i(t) - \omega_i a_i^2(t) - \dot{\alpha}_i(\cdot) \\ &\quad -\Psi_i\theta_i^{*T}\zeta_i(\mathbf{x})\big) + \Psi_i|\tilde{\sigma}_i(t)|\varepsilon_{\max,i} - G_i\tilde{\sigma}_i(t)\eta_{\min,i}\hat{u}_i(t) \\ &\quad + \tilde{\sigma}_i(t)c_{2,i}\big(-c_{1,i}z_{1,i} + \varrho_i\rho_i z_{2,i}\big) \end{aligned} \tag{46}$$

Consider the arc-tangent-based compound reaching law proposed in Ref. [52] as

$$\dot{\tilde{\sigma}}_i(t) = -\beta_{1,i}\arctan\big(\beta_{2,i}|\tilde{\sigma}_i(t)|\big)\mathrm{sign}(\tilde{\sigma}_i(t)) - \beta_{3,i}\tilde{\sigma}_i(t) \tag{47}$$

where $\beta_{1,i}$, $\beta_{2,i}$, and $\beta_{3,i}$ are positive design constants, sign(·) denotes the signum or sign function. Figure 4 compares the proposed reaching law and sliding surface with other most common ones. The convergence speed for the corresponding reaching laws from $\tilde{\sigma}(0) = 1$ can be seen in Fig. 4(*a*).

We design the control input $\hat{u}_i(t)$ as

$$\begin{aligned} \hat{u}_i(t) = (\Psi_i\eta_{\min,i}G_i)^{-1}\big(\varrho_i\rho_i z_{1,i}(t) + a_{i-1}(t) - a_i(t)\omega_i a_i^2(t) \\ + \Psi_i\hat{\theta}_i^T\zeta_i(\mathbf{x}) - \dot{\alpha}_i(\cdot) + c_{2,i}(-c_{1,i}z_{1,i} + \varrho_i\rho_i z_{2,i}) \\ +\beta_{1,i}\arctan\big(\beta_{2,i}|\tilde{\sigma}_i(t)|\big)\mathrm{sign}(\tilde{\sigma}_i(t)) + \beta_{3,i}\tilde{\sigma}_i(t)\big) \end{aligned} \tag{48}$$

The adaptive law for the parameter vector $\hat{\boldsymbol{\theta}}_i$ is given as

$$\dot{\hat{\theta}}_i = -\gamma_{\theta,i}\Psi_i\tilde{\sigma}_i(t)\boldsymbol{\zeta}_i(\mathbf{x}) - \phi_{\theta,i}\hat{\theta}_i \tag{49}$$

where $\gamma_{\theta,i}$ and $\phi_{\theta,i}$ are positive design constants.

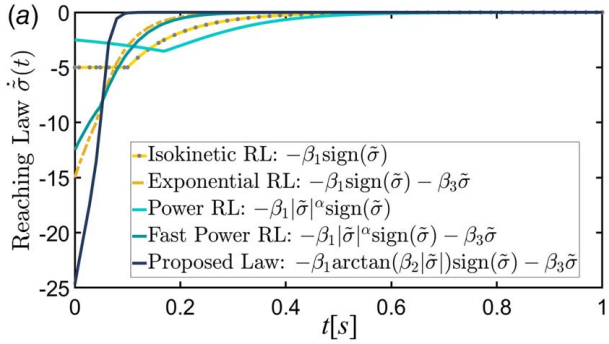

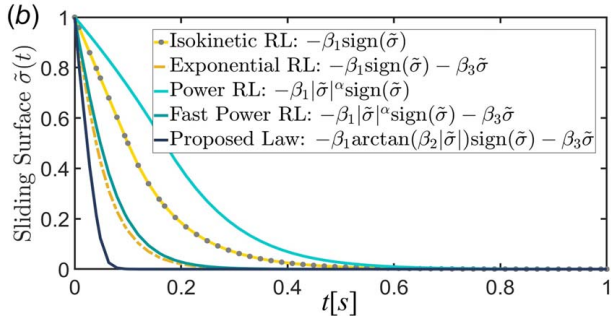

Fig. 4 Comparison of commonly used reaching laws (*a*) and the corresponding sliding surfaces (*b*) ($\beta_1 = 10$, $\beta_2 = 10$, $\beta_3 = 10$, $\alpha = 0.5$)

4.2 Stability Analysis

THEOREM 1. *A plant dynamics defined in (9)–(11) with an actuator fault as in (8) and designed PPC-based BSMC (48) and the adaptive law of the IT2FLS (49) with the earlier predefined assumptions can be stabilized as the error $e_i(t)$ guaranteed to be ultimately bounded in the prescribed small error range near zero as defined in (27).*

Proof. Design the following Lyapunov candidate function as

$$V_{2,i}(t) = V_{1,i}(t) + \frac{1}{2}\tilde{\sigma}_i^2(t) + \frac{1}{2\gamma_{\theta,i}}\tilde{\theta}_i^T\tilde{\theta}_i \tag{50}$$

where $\tilde{\theta}_i = \hat{\theta}_i - \theta_i^*$ denotes a parameter vector approximation error. Taking the derivative of Eq. (50) with respect to time gives

$$\dot{V}_{2,i}(t) = \dot{V}_{1,i}(t) + \tilde{\sigma}_i(t)\dot{\tilde{\sigma}}_i(t) + \frac{1}{\gamma_{\theta,i}}\tilde{\theta}_i^T\dot{\tilde{\theta}}_i \tag{51}$$

For a constant θ_i^*, we have $\dot{\theta}_i^* = 0$. Differentiating the approximating error gives

$$\dot{\tilde{\theta}}_i = \dot{\hat{\theta}}_i - \dot{\theta}_i^* = \dot{\hat{\theta}}_i \tag{52}$$

Plugging Eqs. (44), (52), and (39) into (51) yields

$$\begin{aligned} \dot{V}_{2,i}(t) = -c_{1,i}z_{1,i}^2 + \varrho_i\rho_i z_{1,i}(t)z_{2,i}(t) + \tilde{\sigma}_i(t)(a_{i-1}(t) - a_i(t) \\ -\omega_i a_i^2(t) - \dot{\alpha}_i(\cdot) - \Psi_i\theta_i^{*T}\zeta_i(\mathbf{x})\big) + \Psi_i|\tilde{\sigma}_i(t)|\varepsilon_{\max,i} \\ - G_i\tilde{\sigma}_i(t)\eta_{\min,i}\hat{u}_i(t) + \tilde{\sigma}_i(t)c_{2,i}\big(-c_{1,i}z_{1,i}(t) \\ + \varrho_i\rho_i z_{2,i}(t)\big) + \frac{1}{\gamma_{\theta,i}}\tilde{\theta}_i^T\dot{\hat{\theta}}_i \end{aligned} \tag{53}$$

We have $z_{2,i}(t) = \tilde{\sigma}_i(t) - c_{2,i}z_{1,i}(t)$ from Eq. (36). Thus, we get

$$\begin{aligned} \dot{V}_{2,i}(t) = -c_{1,i}z_{1,i}^2(t) - c_{2,i}\varrho_i\rho_i z_{1,i}^2(t) + \tilde{\sigma}_i\big(\varrho_i\rho_i z_{1,i}(t) \\ + a_{i-1}(t) - a_i(t) - \omega_i a_i^2(t) - \dot{\alpha}_i(\cdot) - \Psi_i\theta_i^{*T}\zeta_i(\mathbf{x})\big) \\ + \Psi_i|\tilde{\sigma}_i(t)|\varepsilon_{\max,i} - G_i\tilde{\sigma}_i(t)\eta_{\min,i}\hat{u}_i(t) \\ + \tilde{\sigma}_i(t)c_{2,i}\big(-c_{1,i}z_{1,i}(t) + \varrho_i\rho_i z_{2,i}(t)\big) + \frac{1}{\gamma_{\theta,i}}\tilde{\theta}_i^T\dot{\hat{\theta}}_i \end{aligned} \tag{54}$$

Plugging the designed control term in Eq. (48) into Eq. (54) and rearranging yields

$$\begin{aligned}\dot{V}_{2,i}(t) = &- c_{1,i}z_{1,i}^2(t) - c_{2,i}\varrho_i\rho_i z_{1,i}^2(t) - \beta_{3,i}\tilde{\sigma}_i^2(t)\\ &+ \Psi_i\tilde{\sigma}_i(t)\tilde{\theta}_i^T\zeta_i(\mathbf{x}) + \frac{1}{\gamma_{\theta,i}}\tilde{\theta}_i^T\dot{\hat{\theta}}_i\\ &- \beta_{1,i}\arctan(\beta_{2,i}|\tilde{\sigma}_i(t)|)|\tilde{\sigma}_i(t)| + \Psi_i|\tilde{\sigma}_i(t)|\varepsilon_{\max,i}\end{aligned} \tag{55}$$

Inserting the adaptive law (49) into (55) and appropriately choosing $\beta_{1,i} \geq \varepsilon_{\max,i}$ yields

$$\dot{V}_{2,i}(t) \leq -c_{1,i}z_{1,i}^2(t) - c_{2,i}\varrho_i\rho_i z_{1,i}^2(t) - \beta_{3,i}\tilde{\sigma}_i^2(t) - \frac{\phi_{\theta,i}}{\gamma_{\theta,i}}\tilde{\theta}_i^T\hat{\theta}_i \tag{56}$$

The following inequality holds:

$$\begin{aligned}-\frac{\phi_{\theta,i}}{\gamma_{\theta,i}}\tilde{\theta}_i\hat{\theta}_i &\leq -\frac{\phi_{\theta,i}}{2\gamma_{\theta,i}}\tilde{\theta}_i^T\tilde{\theta}_i + \frac{\phi_{\theta,i}}{2\gamma_{\theta,i}}\theta_i^{*T}\theta_i^*\\ &\leq -\frac{\phi_{\theta,i}}{2\gamma_{\theta,i}}\|\tilde{\theta}_i\|^2 + \frac{\phi_{\theta,i}}{2\gamma_{\theta,i}}\|\theta_i^*\|^2\end{aligned} \tag{57}$$

Replacing the inequality (57) into (56) and rearranging gives

$$\begin{aligned}\dot{V}_{2,i}(t) \leq &-(c_{1,i} + c_{2,i}\varrho_i\rho_i(t))z_{1,i}^2(t) - \beta_{3,i}\tilde{\sigma}_i^2(t) - \frac{\phi_{\theta,i}}{2\gamma_{\theta,i}}\|\tilde{\theta}_i\|^2\\ &+ \frac{\phi_{\theta,i}}{2\gamma_{\theta,i}}\|\theta_i^*\|^2\end{aligned} \tag{58}$$

Therefore, one can get

$$\dot{V}_{2,i}(t) \leq -\Upsilon_i V_{2,i}(t) + \Gamma_i \tag{59}$$

where

$$\begin{aligned}V_{2,i}(t) &= \frac{1}{2}z_{1,i}^2(t) + \frac{1}{2}\tilde{\sigma}_i^2(t) + \frac{1}{2\gamma_{\theta,i}}\tilde{\theta}_i^T\tilde{\theta}_i\\ \Upsilon_i &=: \min\{2(c_{1,i} + c_{2,i}\varrho_i\rho_i(t)),\ 2\beta_{3,i},\ \phi_{\theta,i}\}\\ \Gamma_i &= \frac{\phi_{\theta,i}}{2\gamma_{\theta,i}}\|\theta_i^*\|^2\end{aligned}$$

Appropriately choosing the design parameters $c_{1,i}$, $c_{2,i}$, $\beta_{1,i}$, $\beta_{2,i}$, $\beta_{3,i}$, $\phi_{\theta,i}$, we have $V_{2,i}(t) \in \mathcal{L}_\infty$ or uniformly ultimately bounded. Therefore, according to Lemma 2, we have

$$0 \leq V_{2,i}(t) \leq \left(V_{2,i}(0) - \frac{\Gamma_i}{\Upsilon_i}\right)e^{-\Upsilon_i t} + \frac{\Gamma_i}{\Upsilon_i} \tag{60}$$

$$\leq V_{2,i}(0) + \frac{\Gamma_i}{\Upsilon_i} \tag{61}$$

Hence, the system tracking error be $\|z_{1,i}(t)\| \leq \sqrt{2\Gamma_i/\Upsilon_i}$. This means that $e_i(t) \in \mathcal{L}_\infty$ is ultimately bounded and could converge to a prescribed asymmetric error bound, which is a small neighborhood of zero $\mathrm{O}_{e_i} := \{-\rho_{s,i}\delta_{\min,i} < e_i(t) < \rho_{s,i}\delta_{\max}\}$ within a predefined settling time t_s at a prescribed converging rate $\left((t_s - t)/t_s\right)^4 w^{-1}(t)$. As a result, the sliding surface $\tilde{\sigma}_i(t)$ in Eq. (36) will be ultimately bounded and can converge to zero due to the proposed reaching law in Eq. (47). This proves that the entire platoon system is string stable and that individual vehicles have stability. This completes the proof. ■

Remark 2. The involvement of the fuzzy approximation system causes the difficulty of proving the asymptotic convergence of the tracking error to zero. Additionally, achieving improved transient performance in the $\mathcal{L}_2$-norm is challenging with the fuzzy system. However, this problem was addressed in Ref. [53] to improve the transient performance of the overall system and achieve asymptotic stability.

To establish strong string stability, we must carefully define the transient performance parameters $\delta_{\max,i}$ and $\delta_{\min,i}$ (as referenced in the prescribed error constraint). We also set $\rho_{s,1} > \rho_{s,2} \geq \cdots \geq \rho_{s,N-1} > \rho_{s,N} \geq 0$, ensuring the condition $e_N(t) \leq e_{N-1}(t) \leq \cdots \leq e_2(t) \leq e_1(t)$ is met. This approach guarantees

$$\pi_i(t) = \frac{|e_{i+1}(t)|}{|e_i(t)|} \leq 1$$

Hence, this prevents the propagation of transient spacing errors across the vehicle platoon. Consequently, the platoon maintains stability as the errors do not amplify.

5 Demonstrative Example

To demonstrate the robustness of the proposed algorithm, a simulation study was performed in MATLAB/Simulink for four AVs in the platoon with homogeneous features following one human-driven vehicle. The initial positions of the vehicles are $\mathbf{p}(0) = [100, 90, 80, 70, 60]^T$m, and the initial velocity and acceleration of all vehicles are 0. The velocity profile for the lead vehicle in m/s is given as

$$v_0(t) = \begin{cases} 2t, & 0 \leq t < 10\\ 20, & 10 \leq t < 25\\ -1.5t + 57.5, & 25 \leq t < 30\\ 12.5, & 30 \leq t < 50\end{cases} \tag{62}$$

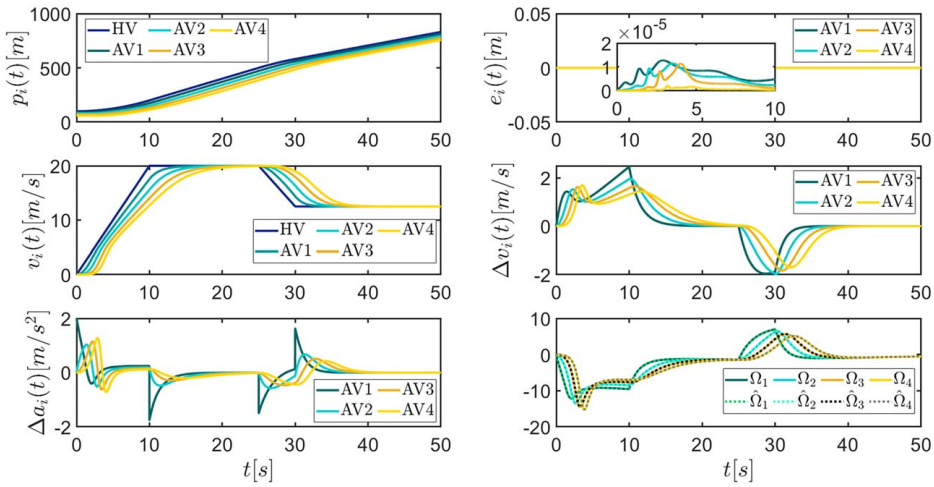

Fig. 5 Control performance under a no-fault condition

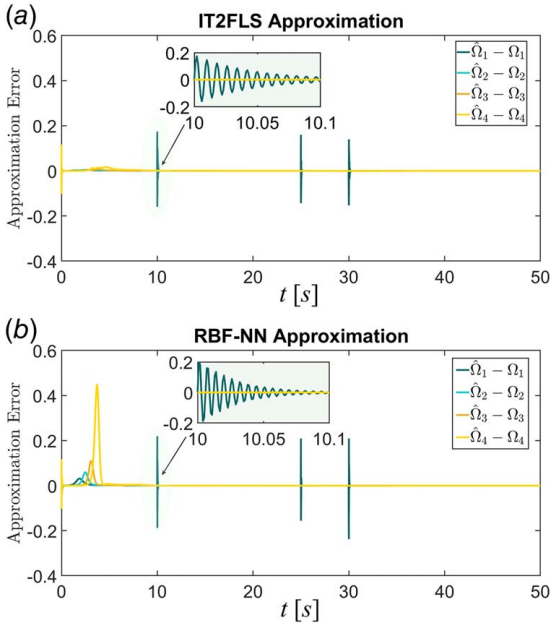

Fig. 6 Comparison of the approximation errors: (*a*) approximation error of IT2FLS and (*b*) approximation error of RBF-NN

The disturbance is $d_i(t) = 0.4\cos(0.1t) + 0.7\sin(0.01t)\,\mathrm{m/s^3}$. The vehicle parameters $m_i = 1450\,\mathrm{kg}$, $\tau_i = 0.2\,\mathrm{s}$, $\rho' = 1.184\,\mathrm{kg/m^3}$, $C_{d,i} = 0.34$, $d_{m,i} = 150\,\mathrm{N}$, and $A_{f,i} = 2.3\,\mathrm{m^2}$. The parameters for the spacing policy are $l_{i-1} = 5\,\mathrm{m}$, $d_{o,i} = 5\,\mathrm{m}$, $\vartheta_i = 0.4$, $a_{\max} = 5\,\mathrm{m/s^2}$, $\kappa_{1,i} = 2.5$, and $\kappa_{2,i} = 2$. The parameters for the controller are $w_i(t) = e^t$, $t_s = 5s$, $\delta_{\max,i} = 1.5$, $\delta_{\min,i} = 1$, $\rho_{s,1} = 0.1$, $\rho_{s,2} = 0.08$, $\rho_{s,3} = 0.05$, $\rho_{s,4} = 0.01$, $c_{1,i} = 1$, $c_{2,i} = 1$, $\beta_{1,i} = 100$, $\beta_{2,i} = 5$, $\beta_{3,i} = 10$, $\phi_{\theta,i} = 1.5$, and $\gamma_{\theta,i} = 1.2 \times 10^6$. For the IT2FLS, five Gaussian MFs with uncertain standard deviation and fixed mean values were designed. The inputs to the IT2FLS are the vehicle's velocity and acceleration. Thus, $\mathbf{x} = [x_1, x_2]^T = [v_i(t), a_i(t)]^T$. Considering the range of these values, i.e., velocity (0–25 m/s) and acceleration (-3.0 to $3.0\,\mathrm{m/s^2}$), we formulate the Gaussian membership functions as in Eq. (19) for the $n = 2$ inputs with $\sigma_1^{s_1} \in [\underline{\sigma}_1^{s_1}, \overline{\sigma}_1^{s_1}]$ and $\sigma_2^{s_2} \in [\underline{\sigma}_2^{s_2}, \overline{\sigma}_2^{s_2}]$ as uncertain standard deviations of input 1 and 2, respectively. We considered an uncertainty of $\pm 1\,\mathrm{m/s}$ and $\pm 0.2\,\mathrm{m/s^2}$ in the velocity and acceleration values, respectively. We designed the means as $\hat{m}_1^{s_1} = [0, 7.5, 15, 22.5, 30]^T$ and $\hat{m}_2^{s_2} = [-3, -1.5, 0, 1.5, 3]^T$ and the uncertain standard deviations are $\sigma_1^{s_1} = 3 \pm 1$ and $\sigma_2^{s_2} = 0.5 \pm 0.2$.

5.1 Simulation Without Fault Condition. We have shown the proposed control scheme under a no-fault condition as in Fig. 5. According to the proposed spacing policy, all the vehicles have achieved string stable conditions from the plot of $e_i(t)$. During the first 5 s, it is noticeable that the velocity difference $\Delta v_i(t)$ and acceleration difference $\Delta a_i(t)$ values will propagate to achieve the preset steady-state error under the proposed exponential spacing policy and the tracking error will converge to zero as the vehicle keeps a constant speed. The bottom right plot shows that the IT2FLS could approximate the unknown nonlinear terms with minimal error. Figure 6 illustrates the comparison of approximation errors of IT2FLS and RBF-NN. For RBF-NN, the adaptive law for the weights is similar as in Eq. (49) with the ζ^T given as

$$\zeta_s = \exp\left(-\frac{\|\mathbf{x} - \hat{\mathbf{m}}_k^s\|^2}{2\left(\boldsymbol{\sigma}_k^s\right)^2}\right), \quad k = 1, 2 \quad \text{and} \quad s = 1, 2, \ldots, h$$

where

$$\hat{\mathbf{m}}_k^s = \begin{bmatrix} \hat{\mathbf{m}}_1^s \\ \hat{\mathbf{m}}_2^s \end{bmatrix} = \begin{bmatrix} 0 & 7.5 & 15 & 22.5 & 30 \\ -3 & -1.5 & 0 & 1.5 & 3 \end{bmatrix}$$

and

$$\boldsymbol{\sigma}_k^s = \begin{bmatrix} \boldsymbol{\sigma}_1^s \\ \boldsymbol{\sigma}_2^s \end{bmatrix} = \begin{bmatrix} 3 & 3 & 3 & 3 & 3 \\ 0.5 & 0.5 & 0.5 & 0.5 & 0.5 \end{bmatrix}$$

From Fig. 6(*a*), we can observe that the IT2FLS achieved less approximation error ($\lesssim 0.2$) than RBF-NN as in Fig. 6(*b*) in which the error surpasses 0.4.

5.2 Simulation With Actuator Fault Condition. Next, we performed a simulation to see the effect of an actuator fault on the robustness of the proposed control strategy. The actuator efficiency is given by a relation as $\eta_i(t) = 0.75 + 0.25\exp(-0.3t)$ and the additive fault is $u_{f,i}(t) = -150(1 - \exp(-0.1t))$. We set $\eta_{\min,i} = 0.75$ and we modify the reaching law parameters $\beta_{1,i} = 200$, $\beta_{2,i} = 5$, and $\beta_{3,i} = 60$. Figure 7 shows the state of the vehicles and the approximation performances under the multiplicative and additive fault conditions. Moreover, we have added white noise and the disturbance $d_i(t)$ equivalent to the one given earlier.

The proposed controller ensured string stability even in the presence of faults and disturbances. It demonstrated comparable tracking performance to that in fault-free conditions. Apart from such tracking performance, the approximation of the unknown terms Ω_i has shown a slight deviation in the first 10 s. The controller regains the performance after 10 s as the approximation error

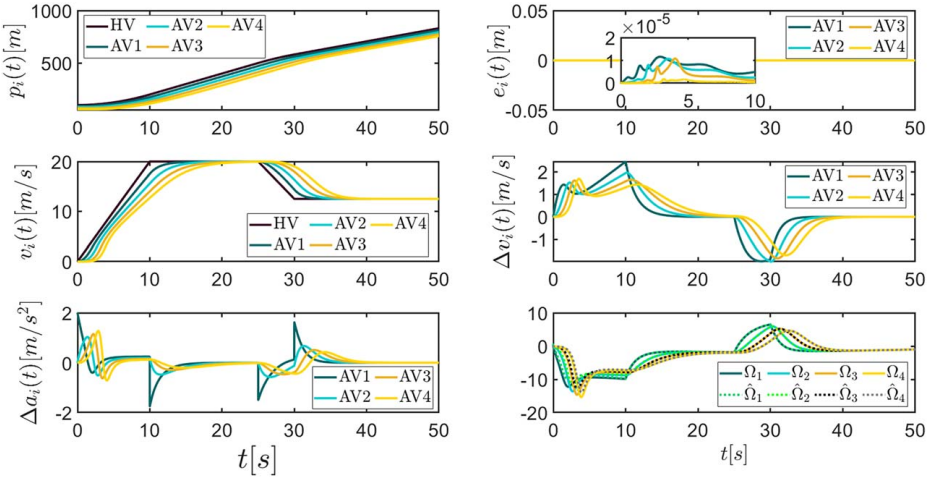

Fig. 7 Control performance under a multiplicative and additive fault condition

approaches almost zero. For the first 5 s, the vehicles will exert higher effort as we move to the tail of the platoon string. This perturbation stabilizes over time, ensuring a stable formation. Sudden variations in the lead vehicle's speed impact the sliding surface profile of the first vehicle, resulting in minor disturbances persisting in the others due to white noise. Additionally, the introduced reaching law successfully eliminated chattering in the signal.

6 Conclusion

In this paper, we designed a backstepping and sliding mode control for an automated platoon experiencing a multiplicative and additive fault. We proposed a prescribed time performance function to bind the position error in a specified margin with a preset speed to achieve string stability. Moreover, we proposed an ESP that considers road and environmental factors to achieve stable operation and vehicular constraints. We proposed an IT2FLS to approximate the unknown nonlinear terms. Finally, the simulation result demonstrated the robustness and performance of the proposed control approach. Besides the discussed practical and positive implications of the control strategy, we can have a few practical challenges while implementing the algorithm. These practical challenges are computational complexity, tuning and calibration, scalability, and integration with existing systems. Implementing IT2FLS and BSMC can be computationally intensive, requiring powerful onboard processing units to perform real-time calculations. Besides, the system's performance heavily depends on accurately tuning fuzzy logic membership functions and control parameters, which can be challenging and time-consuming. Ensuring consistent performance across many vehicles in a platoon might be difficult, especially under varying traffic conditions and external disturbances. Adapting the proposed strategy to work seamlessly with existing vehicle control systems and communication protocols can pose significant integration challenges. Moreover, some future work could be extended. Exploring scenarios involving intermittent sensor delays, communication disruptions, and nonlinear actuator dead zones could be considered. Employing advanced learning algorithms for intelligent parameter tuning is another potential area. Addressing challenges related to vehicle cut-ins in mixed-traffic settings also presents an interesting problem for investigation.

Acknowledgment

The Graduate School Fellowship, Texas Tech University, partly supported this study.

Conflict of Interest

There are no conflicts of interest.

Data Availability Statement

The authors attest that all data for this study are included in the paper.

Appendix A: Vehicle Model Derivation

The summation of all the forces along the longitudinal direction is given by

$$\begin{aligned} m_i a_i(t) &= F_{t,i} - F_{a,i} - d_{m,i} \\ &= F_{t,i} - \frac{1}{2}\rho C_{d,i} A_{f,i} v_i^2(t) - d_{m,i} \end{aligned} \tag{A1}$$

where m_i is the mass of vehicle i, a_i is vehicle acceleration, $F_{t,i}$ is the engine traction force of vehicle i, $F_{a,i}$ is the aerodynamic drag force on vehicle i, ρ is the air density, $C_{d,i}$ is the coefficient of aerodynamic drag, $A_{f,i}$ is the frontal cross-sectional area of vehicle i, v_i is the velocity of vehicle i, and $d_{m,i}$ is the mechanical drag on vehicle i.

Dividing Eq. (A1) by m_i, the acceleration is given as

$$a_i(t) = \frac{1}{m_i}\left(F_{t,i} - \frac{1}{2}\rho C_{d,i} A_{f,i} v_i^2(t) - d_{m,i}\right) \tag{A2}$$

The engine dynamics equation can be expressed as

$$\dot{F}_{t,i}(t) = \frac{1}{\tau_i}\left(-F_{t,i} + u_i(t)\right) \tag{A3}$$

where τ_i is the engine/brake lag time of vehicle i and $u_i \in \mathbb{R}^1$ is the control input to the ith vehicle engine system ($u_i > 0$ represents throttle input and $u_i < 0$ represents braking input).

Differentiating Eq. (A2) yields

$$\dot{a}_i(t) = \frac{1}{m_i}\left(\dot{F}_{t,i} - \frac{1}{m_i}\rho C_{d,i} A_{f,i} v_i(t) a_i(t)\right) \tag{A4}$$

And substituting (A3) into (A4) will give

$$\dot{a}_i(t) = \frac{1}{m_i}\left(-\frac{F_{t,i}}{\tau_i} + \frac{u_i}{\tau_i} - \frac{1}{m_i}\rho C_{d,i} A_{f,i} v_i(t) a_i(t)\right) \tag{A5}$$

Having the relation of $F_{t,i}$ from Eq. (A2), we can have

$$\begin{aligned} \dot{a}_i(t) = &-\frac{1}{\tau_i}\left[a_i(t) + \frac{1}{2m_i}\rho C_{d,i} A_{f,i} v_i(t)^2 + \frac{d_{m,i}}{m_i}\right] \\ &- \frac{1}{m_i}\rho' C_{d,i} A_{f,i} v_i(t) a_i(t) \end{aligned} \tag{A6}$$

Appendix B: Rolle's Theorem

Let $\mathcal{F}$ be a continuous function over the closed interval $[a, b]$ and differentiable over the open interval (a, b) such that $\mathcal{F}(a) = f(b)$. There then exists at least one $\iota \in (a, b)$ such that $\mathcal{F}'(c) = 0$.

Proof. Let $\overline{\varrho} = \mathcal{F}(a) = \mathcal{F}(b)$. We consider three cases:

- $\mathcal{F}(x) = \overline{\varrho}\ \forall x \in (a, b)$.
- There exists $x \in (a, b)$ such that $\mathcal{F}(x) > \overline{\varrho}$.
- There exists $x \in (a, b)$ such that $\mathcal{F}(x) < \overline{\varrho}$.

Case 1. If $\mathcal{F}(x) = \overline{\varrho}$ for all $x \in (a, b)$, then $\mathcal{F}'(x) = 0$ for all $x \in (a, b)$.

Case 2. Since $\mathcal{F}$ is a continuous function over the closed, bounded interval $[a, b]$, according to the extreme value theorem, it has an absolute maximum. Also, since there is a point $x \in (a, b)$ such that $\mathcal{F}(x) > \overline{\varrho}$, the maximum is greater than $\overline{\varrho}$. Hence, the maximum value cannot be found at the beginning or end. Consequently, it must be within the $\iota \in (a, b)$ range. Because $\mathcal{F}$ has a maximum at an interior point ι, and $\mathcal{F}$ is differentiable at ι. Thus, based on Fermat's theorem, $\mathcal{F}'(\iota) = 0$.

Case 3. The case when there exists a point $x \in (a, b)$ such that $\mathcal{F}(x) < \overline{\varrho}$ is analogous to case 2, with maximum replaced by minimum. ∎

References

[1] Gao, Z., Wang, J., Dong, J., and Chen, L., 2019, "Traffic Oscillations Mitigation in Vehicle Platoon Using a Car Following Control Model for Connected and Autonomous Vehicle," J. Adv. Transp., **2019**(1), pp. 1–12.

[2] Negash, N. M., and Yang, J., 2023, "Driver Behavior Modeling Toward Autonomous Vehicles: Comprehensive Review," IEEE Access, **11**, pp. 22788–22821. .

[3] Zhang, L., Chen, F., Ma, X., and Pan, X., 2020, "Fuel Economy in Truck Platooning: A Literature Overview and Directions for Future Research," J. Adv. Transp., **2020**(1), pp. 1–10.

[4] Chen, J., Zhou, Y., and Liang, H., 2019, "Effects of ACC and CACC Vehicles on Traffic Flow Based on an Improved Variable Time Headway Spacing Strategy," IET Intell. Transp. Syst., **13**(9), pp. 1365–1373.

[5] Lee, S., Oh, C., and Lee, G., 2019, "Impact of Automated Truck Platooning on the Performance of Freeway Mixed Traffic Flow," J. Adv. Transp., **2021**(1), pp. 1–13.

[6] Feng, S., Zhang, Y., Li, S., Cao, Z., Liu, H., and Li, L., 2019, "String Stability for Vehicular Platoon Control: Definitions and Analysis," Annu. Rev. Control, **47**, pp. 81–97. .

[7] Darbha, S., Konduri, S., and Pagilla, P., 2018, "Benefits of V2V Communication for Autonomous and Connected Vehicles," IEEE Trans. Intell. Transp. Syst., **20**(5), pp. 1954–1963.
[8] Song, J., and Ju, Y., 2020, "Distributed Adaptive Sliding Mode Control for Vehicle Platoon With Uncertain Driving Resistance and Actuator Saturation," Complexity, **2020**(1), pp. 1–12.
[9] Guo, G., and Li, D., 2019, "Adaptive Sliding Mode Control of Vehicular Platoons With Prescribed Tracking Performance," IEEE Trans. Veh. Technol., **68**(8), pp. 7511–7520.
[10] Swaroop, D., and Rajagopal, K., 2001, "A Review of Constant Time Headway Policy for Automatic Vehicle Following," 2001 IEEE Intelligent Transportation Systems. Proceedings (Cat. No. 01TH8585), pp. 65–69, Paper No. 0-7803-7194-1.
[11] Guo, L., Ge, P., and Sun, D., 2020, "Variable Time Headway Autonomous Emergency Braking Control Algorithm Based on Model Predictive Con- Trol," 2020 Chinese Automation Congress (CAC), pp. 1794–1798, Paper No. 20400146.
[12] Zhao, Q., Zheng, H., Kaku, C., Cheng, F., and Zong, C., 2023, "Safety Spacing Control of Truck Platoon Based on Emergency Braking Under Different Road Conditions," SAE Int. J. Veh. Dyn. Stab. NVH, **7**(1), pp. 69–81.
[13] Orosz, G., 2016, "Connected Cruise Control: Modelling, Delay Effects, and Nonlinear Behaviour," Veh. Syst. Dyn., **54**(8), pp. 147–1176.
[14] Sungu, H., Inoue, M., and Imura, I., 2015, "Nonlinear Spacing Policy Based Vehicle Platoon Control for Local String Stability and Global Traffic Flow Stability," 2015 European Control Conference (ECC), pp. 3396–3401, Paper No. 15603914.
[15] Ge, J., and Orosz, G., 2017, "Optimal Control of Connected Vehicle Systems With Communication Delay and Driver Reaction Time," IEEE Trans. Intell. Transp. Syst., **18**(8), pp. 2056–2070.
[16] Xu, L., Zhuang, W., Yin, G., and Bian, C., 2018, "Stable Longitudinal Control of Heterogeneous Vehicular Platoon With Disturbances and Information Delays," IEEE Access, **6**, pp. 69794–69806. .
[17] Ma, G., 2021, "Robust Control and Optimization for Autonomous and Connected Vehicle Platoons With Vehicle-to-Vehicle Communication Delay," J. Transp. Eng. Part A: Syst., **147**(8), p. 04021042.
[18] Hu, J., Bhowmick, P., Arvin, F., Lanzon, A., and Lennox, B., 2020, "Cooperative Control of Heterogeneous Connected Vehicle Platoons: An Adaptive Leader-Following Approach," IEEE Robot. Autom. Lett., **5**(2), pp. 977–984.
[19] Wang, P., Deng, H., Zhang, J., Zhang, M., and Li, Y., 2021, "Model Predictive Control for Connected Vehicle Platoon Under Switching Communication Topology," IEEE Trans. Intell. Transp. Syst., **23**(7), pp. 7817–7830.
[20] Yan, M., Ma, W., Zuo, L., and Yang, P., 2020, "Distributed Model Predictive Control for Platooning of Heterogeneous Vehicles With Multiple Constraints and Communication Delays," J. Adv. Transp., **2020**(1), pp. 1–16.
[21] Xia, Q., Gao, F., Duan, J., and He, Y., 2017, "Decoupled H_∞ Control of Automated Vehicular Platoons With Complex Interaction Topologies," IET Intell. Transp. Syst., **11**(2), pp. 92–101.
[22] Zheng, Y., Li, S., Li, K., and Ren, W., 2018, "Platooning of Connected Vehicles With Undirected Topologies: Robustness Analysis and Distributed H-Infinity Controller Synthesis," IEEE Trans. Intell. Transp. Syst., **19**(5), pp. 1353–1364.
[23] Negash, N. M., and Yang, J., 2022, "Coupled Integral Sliding Mode Control for Bidirectional Automated Platoon With an Exponential Spacing Policy and Uncertainty Approximation," Proceedings of the ASME IDETC/CIE, p. V001T01A005, Paper No. DETC2022-90810.
[24] Wang, W., Han, B., Guo, Y., Luo, X., and Yuan, M., 2020, "Fault-Tolerant Platoon Control of Autonomous Vehicles Based on Event-Triggered Control Strategy," IEEE Access, **8**, pp. 25122–25134.
[25] Bansal, K., and Mukhija, P., 2020, "Event-Triggered Control of Vehicular Platoon System With Time-Varying Delay and Sensor Faults," J. Autom. Eng., **234**(14), pp. 3362–3372.
[26] Prayitno, A., and Nilkhamhang, I., 2021, "Distributed Model Reference Adaptive Control for Vehicle Platoons With Uncertain Dynamics," Eng. J., **25**(8), pp. 3362–3372.
[27] Peng, Y. F., 2010, "Adaptive Intelligent Backstepping Longitudinal Control of Vehicle Platoons Using Output Recurrent Cerebellar Model Articulation Controller," Expert Syst. Appl., **37**(3), pp. 2016–2027.
[28] Chou, F. C., Tang, S. X., Lu, X., and Alexandre, B., 2019, "Backstepping-Based Time-Gap Regulation for Platoons," Proceedings of the ACC, p. V001T01A005, Paper No. 18954864.
[29] Zhu, Y., Wu, J., and Su, H., 2020, "V2v-Based Cooperative Control of Uncertain, Disturbed and Constrained Nonlinear CAVS Platoon," IEEE Trans. Intell. Transp. Syst., **23**(3), pp. 1796–1806.
[30] Kwon, J. W., and Chwa, D., 2014, "Adaptive Bidirectional Platoon Control Using a Coupled Sliding Mode Control Method," IEEE Trans. Intell. Transp. Syst., **15**(5), pp. 2040–2048.
[31] Zuo, L., Yan, Y., Yan, M., and Ma, W., 2020, "Distributed Integral Sliding Mode-Based Nonlinear Vehicle Platoon Control With Quadratic Spacing Policy," Complexity, **2020**(1), pp. 1–9.
[32] Zheng, Y., Li, S. E., Wang, J., Cao, D., and Li, K., 2016, "Stability and Scalability of Homogeneous Vehicular Platoon: Study on the Influence of Information Flow Topologies," IEEE Trans. Intell. Transp. Syst., **17**(1), pp. 1–14.
[33] Yan, M., Song, J., Yang, P., and Zuo, L., 2018, "Neural Adaptive Sliding-Mode Control of a Bidirectional Vehicle Platoon with Velocity Constraints and Input Saturation," Complexity, **2018**(1), pp. 1–11.
[34] Guo, X., Wang, J., Liao, F., and Teo, R., 2018, "Neuroadaptive Quantized PID Sliding-Mode Control for Heterogeneous Vehicular Platoon With Unknown Actuator Deadzone," J. Robust Nonlinear Control, **29**(1), pp. 188–208.
[35] Guo, G., Li, P., and Hao, L., 2018, "A New Quadratic Spacing Policy and Adaptive Fault-Tolerant Platooning With Actuator Saturation," IEEE Trans. Intell. Transp. Syst., **23**(2), pp. 1200–1212.
[36] Guo, G., Li, P., and Hao, L., 2020, "Adaptive Fault-Tolerant Control of Platoons With Guaranteed Traffic Flow Stability," IEEE Trans. Veh. Technol., **69**(7), pp. 6916–6927.
[37] Gao, Z., Zhang, Y., and Guo, G., 2022, "Fixed-Time Prescribed Performance Adaptive Fixed-Time Sliding Mode Control for Vehicular Platoons With Actuator Saturation," IEEE Trans. Intell. Transp. Syst., **23**(12), pp. 24176–24189.
[38] Guo, G., and Li, D., 2019, "Adaptive Sliding Mode Control of Vehicular Platoons With Prescribed Tracking Performance," IEEE Trans. Veh. Technol., **68**(8), pp. 7511–7520.
[39] Ghasemi, A., and Kazemi, R., 2013, "Stable Decentralized Control of a Platoon of Vehicles With Heterogeneous Information Feedback," IEEE Trans. Veh. Technol., **62**(9), pp. 4299–4308.
[40] Li, Y., Zhao, Y., and Tong, S., 2019, "Adaptive Fuzzy Control for Heterogeneous Vehicular Platoon Systems With Collision Avoidance and Connectivity Preservation," IEEE Trans. Fuzzy Syst., **31**(11), pp. 3934–3943.
[41] Wang, H., Chen, B., Lin, C., Sun, Y., and Wang, F., 2017, "Adaptive Finite-Time Control for a Class of Uncertain High-Order Non-linear Systems Based on Fuzzy Approximation," IET Control Theory Appl., **11**(5), pp. 677–684.
[42] Ge, S. S., and Wang, C., 2004, "Adaptive Neural Control of Uncertain MIMO Nonlinear Systems," IEEE Trans. Neural Netw., **15**(3), pp. 674–692.
[43] Rajamani, R., 2008, *Vehicle Dynamics and Control*, Springer, New York.
[44] Liang, Q., and Mendel, J., 2000, "Interval Type-2 Fuzzy Logic Systems: Theory and Design," IEEE Trans. Fuzzy Syst., **8**(5), pp. 535–550.
[45] Chen, Y., and Yang, J., 2021, "Study on Center-of-Sets Type-Reduction of Interval Type-2 Fuzzy Logic Systems With Noniterative Algorithms," J. Intell. Fuzzy Syst., **40**(6), pp. 11099–11106.
[46] Mendel, J. M., 2014, "General Type-2 Fuzzy Logic Systems Made Simple: A Tutorial," IEEE Trans. Fuzzy Syst., **22**(5), pp. 1162–1182.
[47] Nie, M., and Tan, W. W., 2008, "Towards an Efficient Type-Reduction Method for Interval Type-2 Fuzzy Logic Systems," 2008 IEEE International Conference on Fuzzy Systems, pp. 1425–1432, Paper No. 10221820.
[48] Zhao, K., and Song, Y. D., 2019, "Removing the Feasibility Conditions Imposed on Tracking Control Designs for State-Constrained Strict-Feedback Systems," IEEE Trans. Autom. Control, **64**(3), pp. 1265–1272.
[49] Zhou, S., and Song, Y., 2021, "Prescribed Performance Neuroadaptive Fault-Tolerant Compensation for Mimo Nonlinear Systems Under Extreme Actuator Failures," IEEE Trans. Syst. Man Cybern. Syst., **51**(9), pp. 5427–5436.
[50] Zhao, K., Song, Y., Ma, T., and He, L., 2018, "Prescribed Performance Control of Uncertain Euler–Lagrange Systems Subject to Full-State Constraints," IEEE Trans. Neural Netw. Learn. Syst., **29**(8), pp. 3478–3489.
[51] Xue, G., Lin, F., Li, S., and Liu, H., 2021, "Adaptive Dynamic Surface Control for Finite-Time Tracking of Uncertain Nonlinear Systems With Dead-Zone Inputs and Actuator Faults," Int. J. Control Autom. Syst., **19**(8), pp. 2797–2811.
[52] Ba, K., Yu, B., Liu, Y., Jin, Z., Gao, Z., Zhang, J., and Kong, X., 2020, "Fuzzy Terminal Sliding Mode Control With Compound Reaching Law and Time Delay Estimation for HDU of Legged Robot," Complexity, **2020**(1), pp. 1–16.
[53] Lai, G., Zhang, Y., Liu, Z., and Chen, C. L. P., 2019, "Indirect Adaptive Fuzzy Control Design With Guaranteed Tracking Error Performance for Uncertain Canonical Nonlinear Systems," IEEE Trans. Fuzzy Syst., **27**(6), pp. 1139–1150.